Critical Rate for Water Coning: Correlation and Analytical Solution

Leif A. Høyland, SPE, Statoil, and **Paul Papatzacos,** SPE, and **Svein M. Skjaeveland,** SPE, Rogaland U.

SPE 15855

Summary. Two methods are presented for predicting critical oil rate for bottomwater coning in anisotropic, homogeneous formations with the well completed from the top of the formation. The first method is based on an analytical solution where Muskat's assumption of uniform flux at the wellbore has been replaced by that of an infinitely conductive wellbore. The potential distribution in the oil zone, however, is assumed unperturbed by the water cone. The method is derived from a general solution of the time-dependent diffusivity equation for compressible, single-phase flow in the steady-state limit. We show that very little difference exists between our solution and Muskat's. The deviation from simulation results is caused by the cone influence on potential distribution.

The second method is based on a large number of simulation runs with a general numerical reservoir model, with more than 50 critical rates determined. The results are combined in an equation for the isotropic case and in a single diagram for the anisotropic case. The correlation is valid for dimensionless radii between 0.5 and 50 and shows a rapid change in critical rate for values below five. Within the accuracy of numerical modeling results, Wheatley's theory is shown to predict the correct critical rates closely for all well penetrations in the dimensionless radius range from 2 to 50.

Introduction

Oil production from a well that partly penetrates an oil zone overlying water may cause the oil/water interface to deform into a bell shape. This deformation is usually called water coning and occurs when the vertical component of the viscous force exceeds the net gravity force. At a certain production rate, the water cone is stable with its apex at a distance below the bottom of the well, but an infinitesimal rate increase will cause cone instability and water breakthrough. This limiting rate is called the critical rate for water coning.

Muskat and Wyckoff[1] presented an approximate solution of the water-coning problem. For an isotropic reservoir, the critical rate may be estimated from a graph in their work. Their solution is based on the following three assumptions: (1) the single-phase (oil) potential distribution around the well at steady-state conditions is given by the solution of Laplace's equation for incompressible fluid; (2) a uniform-flux boundary condition exists at the well, giving a varying well potential with depth; and (3) the potential distribution in the oil phase is not influenced by the cone shape.

Meyer and Garder[2] simplified the analytical derivation by assuming radial flow and that the critical rate is determined when the water cone touches the bottom of the well. Chaney *et al.*[3] included completions at any depth in a homogeneous, isotropic reservoir. Their results are based on mathematical analysis and potentiometric model techniques. Chierici *et al.*[4] used a potentiometric model and included both gas and water coning. The results are presented in dimensionless graphs that take into account reservoir anisotropy. Also, Muskat and Wyckoff's Assumption 2 is eliminated because the well was represented by an electric conductor. The graphs are developed for dimensionless radii down to five. For thick reservoirs with low ratios between vertical and horizontal permeability, however, dimensionless radii below five are required. Schols[5] derived an empirical expression for the critical rate for water coning from experiments on Hele-Shaw models.

Recently, Wheatley[6] presented an approximate theory for oil/water coning of incompressible fluids in a stable cone situation. Through physical arguments, he postulated a potential function containing a linear combination of line and point sources with three adjustable parameters. The function satisfies Laplace's equation, and by properly adjusting the parameters, Wheatley was able to satisfy the boundary conditions closely, including that of constant well potential. Most important, his theory is the first to take into account the cone shape by requiring the cone surface—i.e., the oil/water interface—to be a streamline. Included in his paper is a fairly simple procedure for predicting critical rate as a function of dimensionless radius and well penetration for general anisotropic formations. Because of the scarcity of published data on correct critical rates, the precision of his theory is insufficiently documented.

Although each practical well problem may be treated individually by numerical simulation, there is a need for correlations in large-gridblock simulators[7] and for quick, reliable estimates of coning behavior.[8]

This paper presents (1) an analytical solution that removes Assumptions 1 and 2 in Muskat and Wyckoff's[1] theory; (2) practical correlations to predict critical rate for water coning based on a large number of simulation runs with a general numerical reservoir model; and (3) a verification of the predictability of Wheatley's theory. All results are limited to a well perforated from the top of the formation.

Analytical Solution

The analytical solution presented in this paper is an extension of Muskat and Wyckoff's[1] theory and is based on the work of Papatzacos.[9,10] Papatzacos developed a general, time-dependent solution of the diffusivity equation for flow of a slightly compressible, single-phase fluid toward an infinitely conductive well in an infinite reservoir. In the steady-state limit, the solution takes a simple form and is combined with the method of images to give the boundary conditions, both vertically and laterally, as shown in Fig. 1 (see the appendix for details). To predict the critical rate, we superimpose the same criteria as those of Muskat and Wyckoff[1] on the single-phase solution and therefore neglect the influence of cone shape on the potential distribution.

A computer program was developed to give the critical rate in a constant-pressure square from Eqs. A-6 through A-13. The length of the square was transformed to an equivalent radius for a constant-pressure circle[11] to conform with the geometry of Fig. 1 and the simulation cases.

The results of the analytical solution are presented in Fig. 2, where dimensionless critical rate, q_{cD}, is plotted vs. dimensionless radius, r_D, for five fractional well penetrations, L_p/h_t, with the definitions

$$q_{cD}=[40{,}667.25\mu_o B_o/h_t^2(\rho_w-\rho_o)k_H]q_c \quad \ldots\ldots\ldots\ldots\ldots (1)$$

and

$$r_D=(r_e/h_t)\sqrt{k_V/k_H} \quad \ldots\ldots\ldots\ldots\ldots\ldots\ldots\ldots\ldots (2)$$

Numerical Simulation

The critical rate was determined for a wide range of reservoir and well parameters by a numerical reservoir model. The purpose was to check the validity of the analytical solutions and to develop separate practical correlations valid to a low dimensionless radius. A summary is presented here; Ref. 12 gives the details.

The numerical model used is a standard, three-phase, black-oil model with finite-difference formulation developed at Rogaland Research Inst. The validity of the model has been extensively tested. It is fully implicit with simultaneous and direct solution and therefore suitable for coning studies.

The reservoir rock and fluid data are typical for a North Sea sandstone reservoir. All simulations were performed above the bubblepoint pressure. Imbibition relative permeability curves were used, and capillary pressure was neglected. Table 1 gives the rock prop-

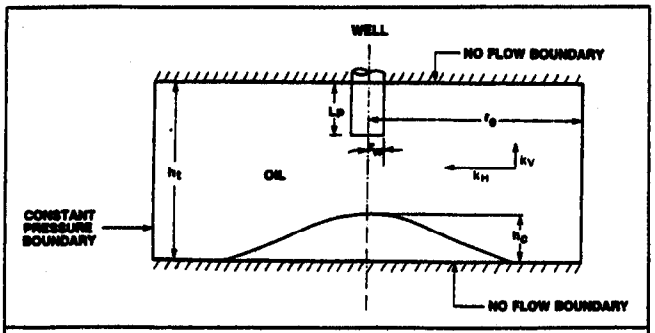

Fig. 1—Partially penetrating well with boundary conditions for analytical solution.

TABLE 1—ROCK PROPERTIES AND FLUID SATURATIONS

Rock Properties	
Rock compressibility, psi $^{-1}$	0.000003
Horizontal permeability, md	1,500
Vertical permeability, md	1,500
Porosity, fraction	0.274
Fluid Saturations	
Interstitial water saturation, fraction	0.170
Residual oil saturation, fraction	0.250

erties and fluid saturations. Tables 2 and 3 give the fluid properties and relative permeabilities, respectively.

Fig. 3 shows the reservoir geometry, boundary conditions, and numerical grid. The water zone is represented by the bottom layer with infinite porosity and permeability to simulate a constant-pressure boundary at the original oil/water contact. The outer radial column with infinite permeability and porosity is included to simulate a constant-pressure outer boundary. To conform with the no-flow boundary at the bottom of the formation in our analytical solution, we could have given the water layer the oil-zone permeability and porosity except for the last column. For a stable cone, however, water pressure at the bottom of the formation is constant and independent of radius. We made our choice to save computer time and obtained the same results for stable cone determination as when the water had to move from the external boundary to establish the cone. Also, as Fig. 3 indicates, the first column of blocks was used to simulate the wellbore to ensure infinite conductivity and correct rate distribution between perforated grid layers.

Many computer runs were made to eliminate numerical grid effects, and we tried to achieve approximately constant potential drop, both horizontally and vertically, between gridblocks at steady-state

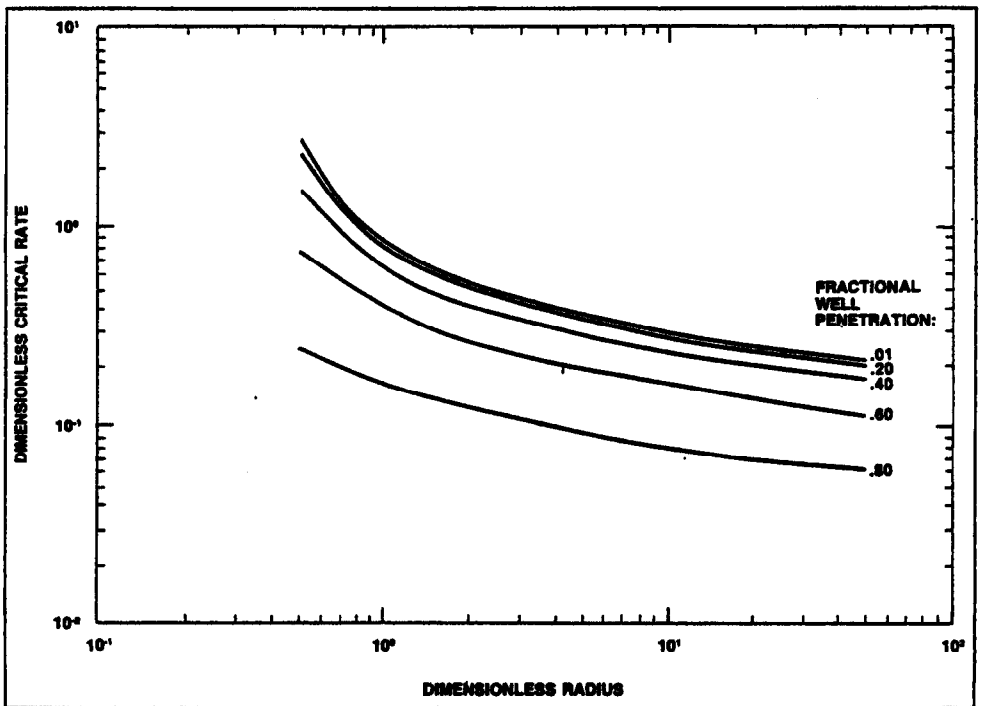

Fig. 2—Critical rate from analytical solution.

TABLE 2—RESERVOIR FLUID PROPERTIES

Oil Properties

Pressure (psia)	FVF (RB/STB)	Solution GOR (scf/STB)	Density (lbm/ft^3)	Viscosity (cp)
1,863.7	1.366	546.0	42.7	0.730
2,573.7	1.449	733.0	41.5	0.660
3,282.7	1.432	733.0	42.0	0.699
4,056.7	1.413	733.0	42.6	0.742
9,500.0	1.281	733.0	47.0	1.042

Water Properties

Viscosity, cp	0.42
Compressibility, psi $^{-1}$	0.000003
FVF, RB/STB	1.03
Density, lbm/ft^3	62.5

conditions. Grid sensitivity runs were repeated whenever reservoir geometry or well penetration were altered.[12]

For a given reservoir geometry, set of parameters, and well penetration, the critical rate was determined within 4% accuracy. The procedure was to bracket the critical rate between a rate that gave a stable cone and a higher rate that gave water breakthrough. About five to six runs were usually necessary to fix each critical rate. More than 500 stimulation runs to steady state were performed in this study.

A base case was chosen, and the effect of each parameter was investigated independently. Table 4 gives the numerical grid for the base case, and Table 5 the reservoir parameters. Table 6 gives a selected summary of the results. Parameters not denoted are at their base values. Sensitivity runs are not listed for parameters with no influence on the critical rate.

In summary, the critical rate for water coning is independent of water permeability, the shape of the water/oil relative permeability curves between endpoints, water viscosity, and wellbore radius. The critical rate is a linear function of oil permeability, density difference, oil viscosity, oil FVF, and a nonlinear function of well penetration, radial extent, total oil thickness, and permeability ratio.

Correlations Based on Simulation Results

Isotropic Reservoir. For those parameters giving a nonlinear relation, the critical rate was assumed to be a function of $1-(L_p/h_t)^2$, h_t^2, and $\ln(r_e)$. Using regression analysis in the same manner as Glasø[13] and including the parameters with a linear relationship, we derived the following correlation:

$$q_c=\frac{k_o(\rho_w-\rho_o)}{10{,}822B_o\mu_o}\left[1-\left(\frac{L_p}{h_t}\right)^2\right]^{1.325}h_t^{2.238}[\ln(r_e)]^{-1.990}. \quad . (3)$$

Anisotropic Reservoir. Several attempts failed to correlate the simulation results into an equation. Instead, the results are summarized in graphical form in Fig. 4, where dimensionless critical rate is plotted vs. dimensionless radius, with the same definitions as in Eqs. 1 and 2, for five different fractional well penetrations. About 40 data points have been used to draw the curves. We consider Fig. 4 the major practical contribution of this paper.

Sample Calculation. Determine the critical rate for water coning from the data in Table 7.

1. Calculate dimensionless radius:

$$\frac{r_e}{h_t}\left(\frac{k_V}{k_H}\right)^{1/2}=\frac{500}{200}\left(\frac{640}{1{,}000}\right)^{1/2}=2.$$

2. Determine dimensionless critical rate for several fractional well penetrations from Fig. 4 for a dimensionless radius of two.

TABLE 3—RELATIVE PERMEABILITY

Water Saturation	Water Relative Permeability	Oil Relative Permeability
0.1700	0.0000	1.0000
0.1800	0.0002	0.9800
0.1900	0.0004	0.9500
0.2000	0.0009	0.8500
0.2500	0.0070	0.6000
0.3000	0.0200	0.4100
0.4000	0.0720	0.1800
0.5000	0.1500	0.0675
0.6000	0.2400	0.0155
0.6500	0.2750	0.0050
0.7000	0.3250	0.0008
0.7500	0.3800	0.0000
0.8500	0.5400	0.0000
0.9000	0.6500	0.0000
1.0000	1.0000	0.0000

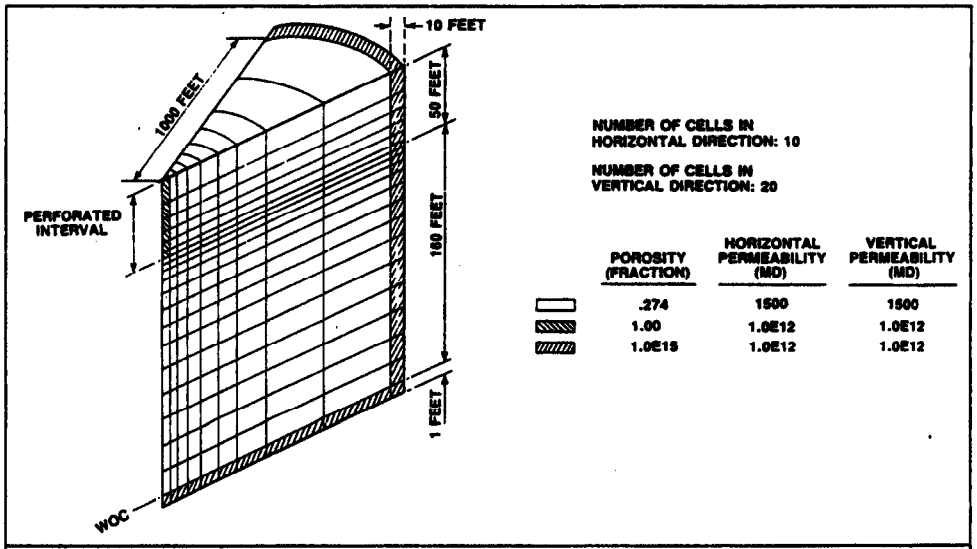

Fig. 3—Sketch of numerical grid.

TABLE 4—GRID SIZE FOR BASE CASE*

Radial block lengths, ft	0.15, 0.45, 1.3, 3.6, 10.5, 29, 81, 229, 645, 10
Vertical block lengths, ft	25, 15.2, 6.3, 2.5, 1, 0.3, 0.5, 0.9, 1.5, 2.5, 4.3, 7.2, 12.3, 20, 20 20, 20, 20, 30.5, 1

*Grid sketched in Fig. 3.

TABLE 5—RESERVOIR PARAMETERS FOR BASE CASE

Fractional well penetration	0.238
Total oil thickness, ft	210
Exterior radius, ft	1,000
Wellbore radius, ft	0.25
Horizontal permeability, md	1,500
Vertical permeability, md	1,500
Oil density, lbm/ft^3	43.6
Oil viscosity, cp	0.826
Oil FVF, RB/STB	1.376
Water properties	Table 2
Relative permeabilities	Table 3
Numerical grid	Table 4

TABLE 6—SUMMARY OF SELECTED SIMULATION CASES

No.	h_t (ft)	r_e (ft)	k_V (md)	L_p/h_t	r_D	q_c (STB/D)	Deviation* (%)
1	210	1,000	1,500	0.048	4.76	7,150	5.2
Base	210	1,000	1,500	0.238	4.76	6,600	4.8
2	210	1,000	1,500	0.476	4.76	5,000	4.8
3	210	1,000	1,500	0.714	4.76	2,700	5.5
4	210	1,000	1,500	0.905	4.76	750	6.0
5	50	1,000	1,500	0.238	20.0	260	12.3
6	100	1,000	1,500	0.238	10.0	1,200	10.7
7	50	1,000	1,500	0.714	20.0	115	6.1
8	210	5,000	1,500	0.476	23.81	3,400	11.2
9	210	500	1,500	0.476	2.38	6,500	−1.9
10	210	500	1,500	0.714	2.38	3,400	0.0
11**	210	1,000	150	0.238	4.76	650	6.3
12**	210	1,000	1,000	0.238	4.76	4,400	4.8
13**	210	1,000	500	0.714	4.76	900	5.4
14	210	1,000	600	0.238	3.01	7,800	0.8
15	210	1,000	150	0.238	1.51	11,000	−8.1
16	210	1,000	37.5	0.238	0.75	20,000	−18.0
17	210	1,000	15	0.238	0.48	42,000	
18	210	1,000	600	0.476	3.01	5,900	0.6
19	210	1,000	60	0.476	0.95	11,100	−15.7
20	210	1,000	15	0.476	0.48	24,000	
21	210	1,000	600	0.714	3.01	3,100	2.9
22	210	1,000	150	0.714	1.51	4,000	−2.4
23	210	1,000	60	0.714	0.95	5,200	−10.1
24	210	1,000	15	0.714	0.48	8,400	13.2
25	210	500	600	0.476	1.51	8,100	−7.4
26	210	500	60	0.476	0.48	24,500	
27	210	500	15	0.476	0.24	118,000	
28	210	5,000	150	0.476	7.53	4,400	7.0
29	210	5,000	37.5	0.476	3.76	5,600	−0.5
30	210	5,000	22.5	0.476	2.92	6,200	−3.4
31	210	5,000	15	0.476	2.38	6,700	−4.8
32	100	1,000	600	0.238	6.32	1,375	6.6
33	100	1,000	60	0.238	2.00	2,100	−2.6
34	100	1,000	15	0.238	1.00	3,400	−16.7
35	50	1,000	600	0.238	12.65	290	9.3
36	50	1,000	60	0.238	4.00	410	0.2
37	50	1,000	15	0.238	2.00	550	−7.1
38	210	500	66.15	0.905	0.5	1,650	−10.4
39	210	500	105,840	0.905	20.0	600	5.8
40	210	500	661,500	0.476	50.0	2,900	16.0
41	210	500	66.15	0.048	0.5	44,000	
42	210	500	105,840	0.048	20	4,800	16.9

*Percentage deviation of corresponding critical rate calculated by Wheatley's method.
**$k_H = k_V$; for all other cases $k_H = 1{,}500$ md.

3. Plot dimensionless critical rate as a function of well penetration, as shown in Fig. 5.
4. Calculate fractional well penetration: $L_p/h_t = 50/200 = 0.25$.
5. Interpolate in the plot in Fig. 5 to find $q_{cD} = 0.375$.
6. Use Eq. 1 and find the critical rate:

$$q_c = \frac{h_t^2(\rho_w - \rho_o)k_H}{40{,}667.25 B_o \mu_o} q_{cD}$$

$$= 5{,}649 \text{ STB/D } [898 \text{ stock-tank m}^3/\text{d}].$$

With the reservoir simulator used independently for the same example, the critical rate was found to be 5,600 STB/D [890 stock-tank m^3/d], determined within 100 STB/D [16 stock-tank m^3/d].

Discussion

Isotropic Reservoir. Fig. 6 shows a comparison between the analytical solutions of Muskat,[14] Papatzacos (presented in this paper), and Wheatley[6] with the correlation of Eq. 3.

The analytical solutions of Muskat and Papatzacos are very close, with a small discrepancy at high well penetrations. They give a higher critical rate (up to 30%) than the correlation. It is obvious that Muskat's solution is not noticeably improved by solving the complete time-dependent diffusivity equation and substituting the uniform-flux wellbore condition with that of infinite conductivity. The shortcomings are caused by the neglect of the cone influence on potential distribution.

The cone influence, however, is taken into account by Wheatley, and the results from his procedure (Fig. 6) are remarkably close to the correlation from a general numerical model, which might be considered the correct solution. In fact, for a dimensionless radius of 2.5, Wheatley's results are within the 4% uncertainty in the critical rates obtained from simulation.

To generate the critical rates from Wheatley's theory, we used his recommended procedure with one exception. Instead of his Eq. 19, which follows from an expansion of his Eq. 18 for large r_D and creates problems when $r_D \to 1$, we used the unexpanded form. The procedure is easily programmed and numerically stable.

The results of several methods to predict critical rate are plotted in Fig. 7 for comparison: the method based on Papatzacos' theory with results close to Muskat's; the correlation from Eq. 3, which is very close to Wheatley's theory; Schols'[5] method based on physical models; and Meyer and Garder's[2] correlation.

General Anisotropic Case. Fig. 8 shows a comparison between the correlation of Chierici *et al.*,[4] the analytical solution based on Papatzacos' theory, and the simulation results for a specific example. The dimensionless critical rate is plotted as a function of dimensionless radius for a fractional well penetration of 0.24. The fully drawn line is based on Papatzacos' theory. The critical rates of Chierici *et al.* are very close to Papatzacos' solution because they rely on essentially the same assumptions. Papatzacos' curve is about 25% above the values determined from numerical simulation. Again,

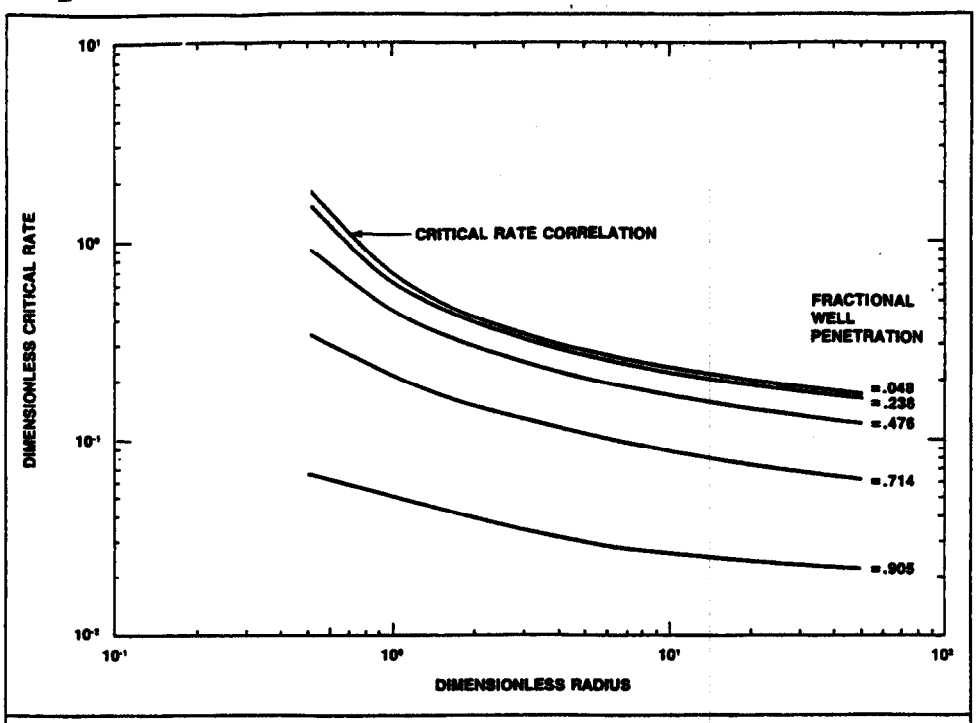

Fig. 4—Critical-rate correlation chart from numerical simulation.

this has to be caused by neglect of cone influence on potential distribution.

Chierici *et al.* developed their diagrams down to a dimensionless radius of five. Values below five are often necessary, however, for North Sea reservoirs. As can be seen from Fig. 8, the critical rate increases dramatically for dimensionless radii below five, and extrapolation of Chierici *et al.*'s diagrams below their validity range may lead to considerable errors.

The critical rates determined from Wheatley's[6] theory are plotted in Fig. 9 on a reproduction of Fig. 4, which represents the cor-

TABLE 7—DATA FOR ANISOTROPIC RESERVOIR SAMPLE CALCULATION

Density difference (water/oil), lbm/ft^3	17.4
Oil FVF, RB/STB	1.376
Oil viscosity, cp	0.8257
Horizontal permeability, md	1,000
Vertical permeability, md	640
Total oil thickness, ft	200
Perforated thickness, ft	50
External radius, ft	500

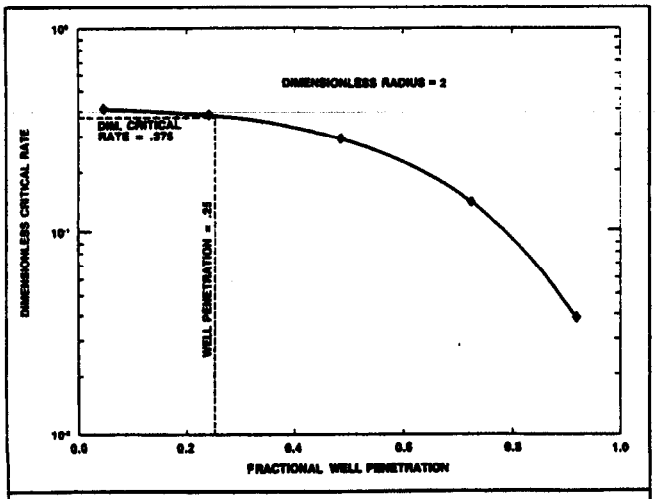

Fig. 5—Critical-rate calculation for example problem.

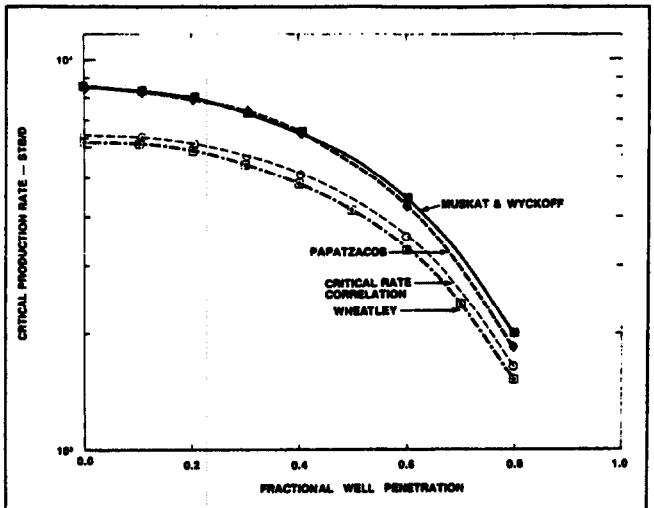

Fig. 6—Critical-rate comparison, isotropic formations.

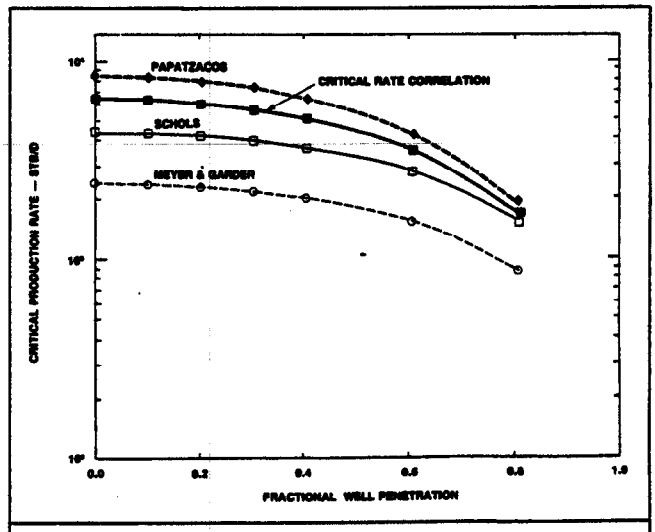

Fig. 7—Critical-rate comparison, isotropic formations.

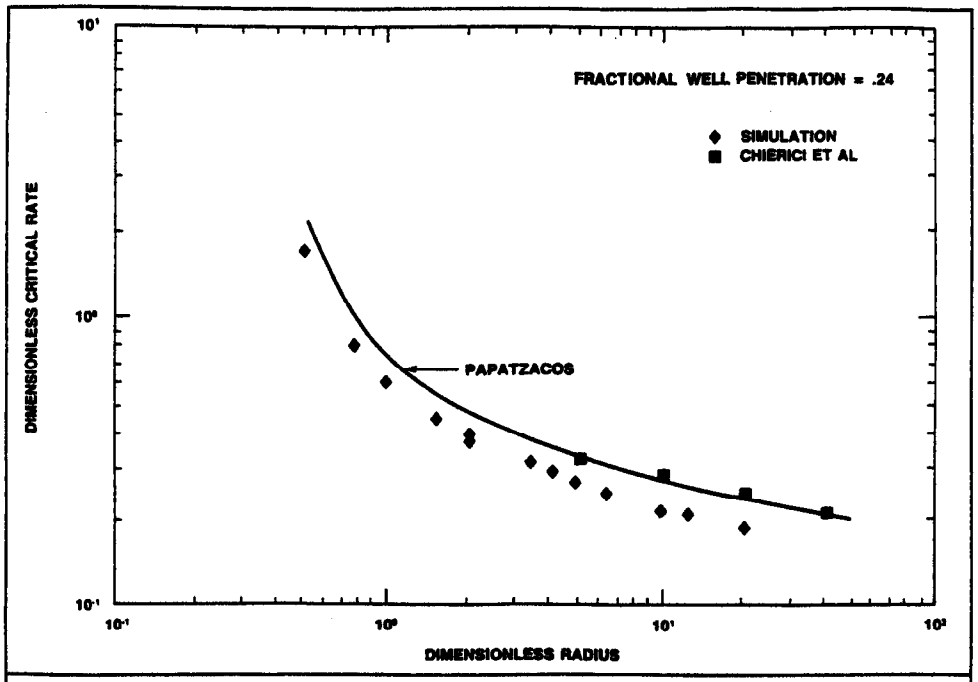

Fig. 8—Critical-rate comparison, anisotropic formations.

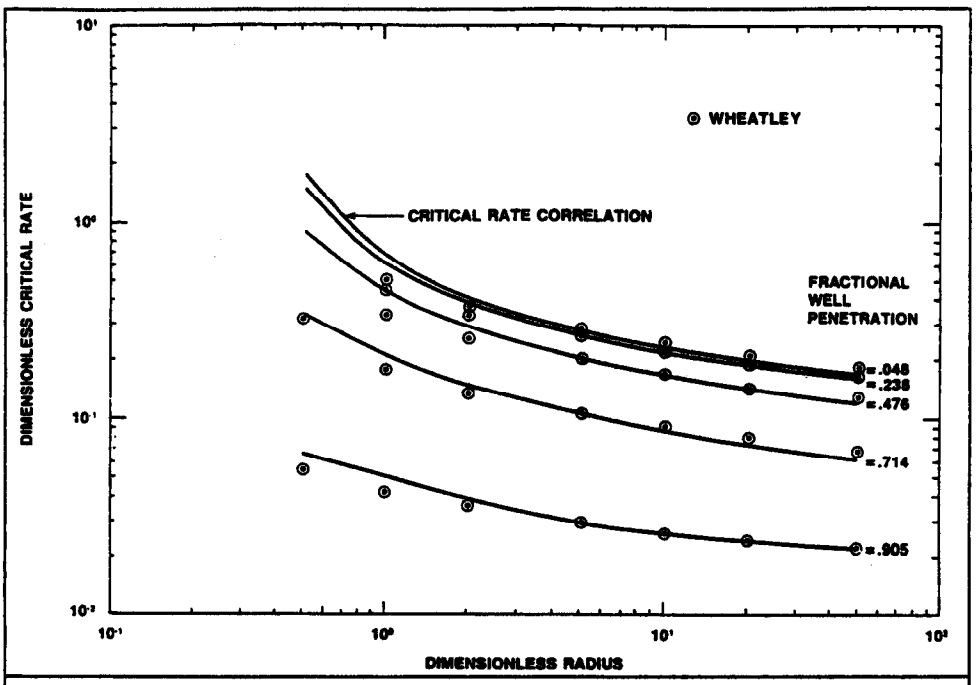

Fig. 9—Critical-rate comparison, anisotropic formations.

rect values from simulation. Also, the last column of Table 6 lists the percentage deviations for the actual cases. The blanks in the column are for low dimensionless radii where Wheatley's theory gave negative critical rates. In these calculations, a fixed dimensionless wellbore radius of 0.002 is used. Checks with actual dimensionless wellbore radii gave nearly identical results.

The accuracy of the critical rates from the simulator is 4%, which is conservative—i.e., the highest rate with a stable cone has been selected. Within this accuracy, Wheatley's theory gives nearly correct critical rates for all well penetrations in the r_D interval from 2 to 50. There is a slight tendency toward high values at the upper end of the interval and toward low values at the lower end.

Critical Cone Height. The critical cone defined by the reservoir simulator was found to stabilize at a certain distance below the well, in accordance with other authors.[5,14] Incremental rate increase caused the water to break abruptly into the well. Fig. 10 shows the dimensionless critical cone height, h_c/h_t, as a function of fractional well penetration for a dimensionless radius of 4.76. The critical cone heights from the analytical solution are fairly close to the simulated results, but no precise conclusion can be drawn because of the coarse vertical resolution in the numerical model.

A straight line drawn in Fig. 10 from the lower right to upper left corners would correspond to the erroneous assumption that the critical cone touches the bottom of the well. As can be seen, the distance between the bottom of the well and the top of the critical cone increases with decreasing well penetration.

Conclusions

1. A general correlation is derived to predict critical rate for water coning in anisotropic reservoirs. The correlation is based on a large number of simulation runs with a numerical model and is present-

ed in a single graph, with dimensionless critical rate as a function of dimensionless radius between 0.5 and 50, at five different well penetrations.

2. For isotropic formations, the correlation is formulated as an equation.

3. A new analytical solution, based on single-phase, compressible fluid and an infinitely conductive wellbore, gives no improvement in critical-rate predictions compared with Muskat's classic solution. The deficiency is caused by neglect of cone influence on the single-phase solution.

4. Within the accuracy of the numerical simulation results, Wheatley's theory closely predicts the correct critical rates for all well penetrations in the dimensionless radius range from 2 to 50.

Nomenclature

B = FVF, RB/STB [res m^3/stock-tank m^3]
C = dimensionless coordinate, Eq. A-7
h_c = critical cone height, distance above original water/oil contact, ft [m]
h_t = total thickness of oil zone, ft [m]
i,j,k = integers, used in Eqs. A-8 through A-10
k_H = horizontal permeability, md
k_o = effective oil permeability, md
k_V = vertical permeability, md
L = length of constant-pressure square, ft [m]
L_p = length of perforated interval, ft [m]
p = pressure, psi [kPa]
q = surface flow rate, STB/D [stock-tank m^3/d]
q_{cD} = dimensionless critical rate, Eqs. 1 and A-13
q_R = reservoir flow rate, RB/D [res m^3/d]
r_e = exterior radius, ft [m]
r_D = dimensionless radius, Eq. 2
Δr_D = radial distance, Eq. A-5, dimensionless
Δr_{ijD} = radial summation coordinate, Eq. A-9, dimensionless
x,y,z = Cartesian coordinates, ft [m]
$x_D, y_D,$
z_D = Cartesian coordinates, Eq. A-1, dimensionless
z_{cD} = critical value of z_D for top of cone, dimensionless
z_{kD} = vertical summation coordinate, Eq. A-10
α,β,ξ = spheroidal coordinates, Eq. A-4, dimensionless
μ = viscosity, cp [mPa·s]
ρ = density, lbm/ft^3 [kg/m^3]
$\Phi = p-\rho_o z/144$, potential, psi [kPa]
Φ_D = dimensionless potential drop, Eq. A-3
Φ'_D = derivative of Φ_D with respect to z_D
$\Phi_D^{(\infty)}$ = steady-state potential drop, perforated interval in reservoir with no boundaries, Eq. A-2, dimensionless
Φ_i = initial reservoir potential, psi [kPa]

Subscripts

c = critical
D = dimensionless
i = initial
o = oil
w = water

Acknowledgments

Parts of this work constitute Høyland's MS thesis at Rogaland U. Centre. He thanks Mobil Exploration Norway Inc. for permission to complete the thesis.

References

1. Muskat, M. and Wyckoff, R.D.: "An Approximate Theory of Water-Coning in Oil Production," *Trans.*, AIME (1935) **114**, 144–61.
2. Meyer, H.I. and Garder, A.O.: "Mechanics of Two Immiscible Fluids in Porous Media," *J. Appl. Phys.* (1954) **25**, No. 11, 1400–06.
3. Chaney, P.E. *et al.*: "How to Perforate Your Well to Prevent Water and Gas Coning," *Oil & Gas J.* (May 7, 1956) 108–14.
4. Chierici, G.L., Ciucci, G.M., and Pizzi, G.: "A Systematic Study of Gas and Water Coning by Potentiometric Models," *JPT* (Aug. 1964) 923–29; *Trans.*, AIME, **231**.
5. Schols, R.S.: "An Empirical Formula for the Critical Oil Production Rate," *Erdoel-Erdgas* (Jan. 1972) 6–11.

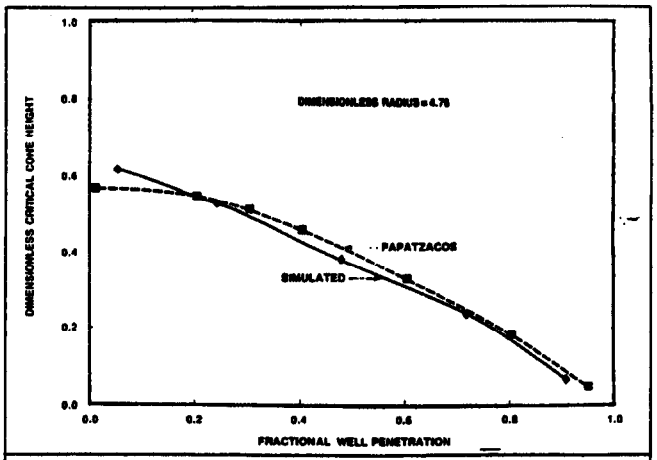

Fig. 10—Critical-cone-height comparison.

6. Wheatley, M.J.: "An Approximate Theory of Oil/Water Coning," paper SPE 14210 presented at the 1985 SPE Annual Technical Conference and Exhibition, Las Vegas, Sept. 22–25.
7. Addington, D.V.: "An Approach to Gas-Coning Correlations for a Large Grid Reservoir Simulator," *JPT* (Nov. 1981) 2267–74.
8. Kuo, M.C.T. and DesBrisay, C.L.: "A Simplified Method for Water Coning Predictions," paper SPE 12067 presented at the 1983 SPE Annual Technical Conference and Exhibition, San Francisco, Oct. 5–8.
9. Papatzacos, P.: "Exact Solutions for Infinite-Conductivity Wells," *SPERE* (May 1987) 217–26; *Trans.*, AIME, **283**.
10. Papatzacos, P.: "Approximate Partial-Penetration Pseudoskin for Infinite-Conductivity Wells," *SPERE* (May 1987) 227–34; *Trans.*, AIME, **283**.
11. Kumar, A. and Ramey, H.J. Jr.: "Well-Test Analysis for a Well in a Constant-Pressure Square," *SPEJ* (April 1974) 107–16.
12. Høyland, L.A.: "Critical Rate for Water Coning in Isotropic and Anisotropic Formations," MS thesis, Rogaland U., Stavanger, Norway (1984).
13. Glasø, Ø.: "Generalized Pressure-Volume-Temperature Correlations," *JPT* (May 1980) 785–95.
14. Muskat, M.: *Physical Principles of Oil Production*, Intl. Human Resources Development Corp. Publishers, Boston, MA (1981).

Appendix—Critical Rate Calculation by Muskat's Method

Muskat's[14] method is used to calculate the critical rate for stable water coning. The method requires an expression for the steady-state potential drop on the axis of the partially penetrating well in terms of the vertical coordinate, with the assumption of constant potential at the lateral boundaries and of no flow across the horizontal boundaries, the lower horizontal boundary being at the original oil/water contact. Such an expression will be obtained here by using the method of images together with an expression for the potential drop owing to an infinite-conductivity well in an infinite reservoir.[9]

Preliminary Equations. The coordinates are the Cartesian (x,y,z), with the z axis pointing downward. The origin is taken at the intersection of the well axis with the upper reservoir boundary (Fig. 1). Dimensionless coordinates are defined as follows.

$$x_D=(k_V/k_H)^{1/2}(x/L_p), \quad \text{(A-1a)}$$

$$y_D=(k_V/k_H)^{1/2}(y/L_p), \quad \text{(A-1b)}$$

and

$$z_D=z/L_p. \quad \text{(A-1c)}$$

To use the method of images, one starts by considering an infinite-conductivity well in an infinite reservoir with no vertical or horizontal boundaries. An interval is open to flow along the above-defined z axis, from $-L_p$ to L_p, and the total reservoir production rate is denoted by $2q_R$. Symmetry implies that no flow takes place across the horizontal plane passing through the middle of the interval open to flow, so that this plane will eventually become the upper reservoir boundary; hence the values of $2L_p$ and $2q_R$. It has been shown by Papatzacos[9] that the potential drop in the steady-state limit for such a well is

$$\Phi_D^{(\infty)}=\tfrac{1}{2}\ \ln[(e^{\xi}+1)/(e^{\xi}-1)], \quad \text{(A-2)}$$

where

$$\Phi_D=(1/141.2)(L_p k_h/2\mu q_R)(\Phi_i-\Phi) \quad \text{(A-3)}$$

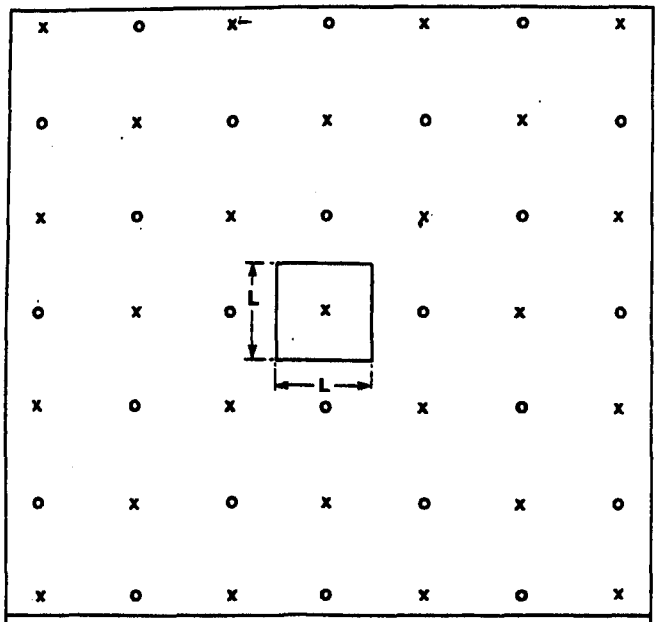

Fig. A-1—Horizontal lattice of production (x) and injection (o) wells.

and where ξ is one of the three spheroidal coordinates (ξ,α,β) defined by

$$x_D=\sinh\xi\sin\alpha\cos\beta, \quad \text{(A-4a)}$$

$$y_D=\sinh\xi\sin\alpha\sin\beta, \quad \text{(A-4b)}$$

and $$z_D=\cosh\xi\sin\alpha. \quad \text{(A-4c)}$$

In view of the cylindrical symmetry, it is useful to introduce

$$\Delta r_D=\sqrt{x_D^2+y_D^2}=\sin\xi\sin\alpha, \quad \text{(A-5)}$$

which is the dimensionless distance from the z axis.

The steady-state potential drop (Eq. A-2) can now be expressed in terms of the more familiar coordinates Δr_D and z_D:

$$\Phi_D^{(\infty)}(\Delta r_D,z_D)=\tfrac{1}{4}\ln[(C+1)/(C-1)], \quad \text{(A-6)}$$

where C is the following function of Δr_D and z_D:

$$C=(1/\sqrt{2})\{1+z_D^2+\Delta r_D^2+[(1+z_D^2+\Delta r_D^2)^2-4z_D^2]^{1/2}\}^{1/2}. \quad \text{(A-7)}$$

Steady-State Potential Drop in a Finite Reservoir. With the method of images, it is now possible to obtain the potential drop in a finite reservoir. The geometry is shown in Figs. A-1 and A-2, where the image wells close to the real well are depicted. The boundary conditions are assumed to be constant potential at the lateral boundaries and no flow through the horizontal boundaries. Constant potential is produced at the lateral boundaries by a horizontal, infinite grid of alternating production and injection wells with the real well at its center (Fig. A-1). No flow at the horizontal boundaries is achieved by an infinite repetition of this grid in the vertical direction (Fig. A-2). Note that advantage is taken of the fact that Eqs. A-2 and A-6 imply that no flow takes place across the horizontal plane passing through the middle of the interval open to flow. The expression for the potential drop on the axis of the real well is

$$\Phi_D(z_D)=\sum_{k=-\infty}^{+\infty}\sum_{j=-\infty}^{+\infty}\sum_{i=-\infty}^{+\infty}(-1)^{i+j}\Phi_D^{(\infty)}(\Delta r_{ijD},z_{kD}), \quad \text{(A-8)}$$

where $\Phi_D^{(\infty)}$ is given by Eqs. A-6 and A-7 and where

$$\Delta r_{ijD}=(i^2+j^2)^{1/2}(k_V/k_H)^{1/2}(L/L_p) \quad \text{(A-9)}$$

and $$z_{kD}=z_D+(2h_t/L_p)k. \quad \text{(A-10)}$$

Although each image well has the infinite-conductivity character, it contributes a potential drop that necessarily varies along the wellbore of the real well so that the method of images does not yield the exact infinite-conductivity solution. Eq. A-8, however, will be a good approximation in most cases of practical interest because Eq. A-6 contributes a constant potential drop along the wellbore of the real well, while the variation caused by the contributions of the image wells is usually small.[10]

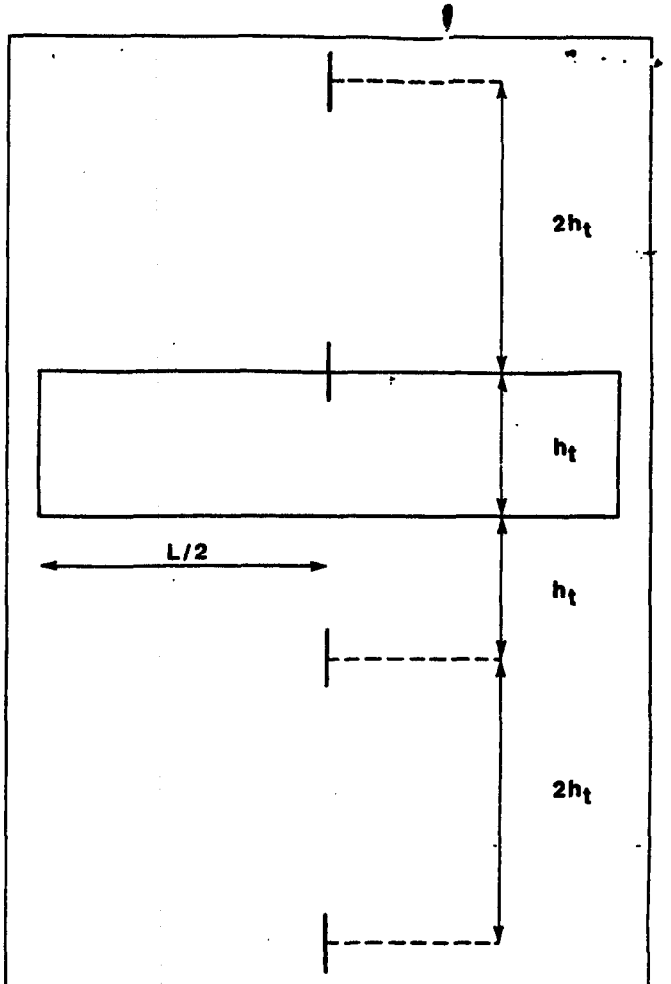

Fig. A-2—Vertical projection of real and image wells.

Critical Rate by Muskat's Method. Muskat assumed that the influence of the cone on the values of Φ_D can be neglected. The static equilibrium condition for a point with vertical coordinate z at the intersection of the cone with the well axis is $\Phi_t(z)-\Phi(z)=(\rho_w-\rho_o)(h_t-z)/144$. This is an equation for z. Considerations of stability[14] show that the only possible values of z are given by the following equation (written in the dimensionless variables of this Appendix):

$$\Phi_D(z_{cD})+\Phi_D'(z_{cD})(h_t/L_p-z_{cD})=0, \quad \text{(A-11)}$$

where Φ_D' is the derivative of Φ_D. This is an equation for z_{cD}, the critical coordinate of the top of the cone. The critical dimensionless rate is then given by

$$q_{cD}=-(L_p/h_t)^2/\Phi_D'(z_{cD}), \quad \text{(A-12)}$$

where $$q_{cD}=[2\times144\times141.2\mu_o/(\rho_w-\rho_o)h_t^2k_H]q_{Rc}. \quad \text{(A-13)}$$

Functions $\Phi_D(z_D)$ and $\Phi_D'(z_D)$ are completely defined by Eqs. A-6 through A-10.

SI Metric Conversion Factors

bbl	× 1.589 873	E−01	= m^3
cp	× 1.0*	E−03	= Pa·s
ft	× 3.048*	E−01	= m
lbm/ft^3	× 1.601 846	E+01	= kg/m^3
md	× 9.869 233	E−04	= μm^2
psi	× 6.894 757	E+00	= kPa
psi^{-1}	× 1.450 377	E−01	= kPa^{-1}
scf/bbl	× 1.801 175	E−01	= std m^3/m^3

*Conversion factor is exact.

SPERE

Original SPE manuscript received for review Sept. 18, 1986. Paper accepted for publication June 28, 1989. Revised manuscript received March 9, 1989. Paper (SPE 15855) first presented at the 1986 SPE European Petroleum Conference held in London, Oct. 20–22.